PHOTONICS Research

High sensitivity *D*-shaped hole fiber temperature sensor based on surface plasmon resonance with liquid filling

Sijun Weng, Li Pei,* Jianshuai Wang, Tigang Ning, and Jing Li

Key Lab of All Optical Network and Advanced Telecommunication Network of Ministry of Education, Institute of Lightwave Technology, Beijing Jiaotong University, Beijing 100044, China
**Corresponding author: lipei@bjtu.edu.cn*

Received 10 October 2016; revised 18 December 2016; accepted 3 January 2017; posted 6 January 2017 (Doc. ID 278394); published 28 February 2017

A high sensitivity *D*-shaped hole double-cladding fiber temperature sensor based on surface plasmon resonance (SPR) is designed and investigated by a full-vector finite element method. Within the *D*-shaped hole double-cladding fiber, the hollow *D*-section is coated with gold film and then injected in a high thermo-optic coefficient liquid to realize the high temperature sensitivity for the fiber SPR temperature sensor. The numerical simulation results show that the peaking loss of the *D*-shaped hole double-cladding fiber SPR is hugely influenced by the distance between the *D*-shaped hole and fiber core and by the thickness of the gold film, but the temperature sensitivity is almost insensitive to the above parameters. When the thermo-optic coefficient is -2.8×10^{-4}/°C, the thickness of the gold film is 47 nm, and the distance between the *D*-shaped hole and fiber core is 5 μm, the temperature sensitivity of the *D*-shaped hole fiber SPR sensor can reach to −3.635 nm/°C.

OCIS codes: (060.2370) Fiber optics sensors; (240.6680) Surface plasmons; (120.6810) Thermal effects.

https://doi.org/10.1364/PRJ.5.000103

1. INTRODUCTION

Temperature sensors based on fiber have been designed and investigated widely in recent years with the advantages of easy remote-control, high temperature sensitivity, electromagnetic wave immunity, and so forth. Kou *et al.*, experimentally demonstrated a fiber temperature sensor based on a first-order fiber grating [1]. Besides, various optical interferometers have been widely applied in the field of fiber sensors as well [2,3]. Accordingly, due to the holey structure, the temperature sensor based on a photonics crystal fiber (PCF) is infiltrated with different kinds of materials to realize the sensing of temperature [4].

Surface plasmon resonance (SPR) has been used in the fiber temperature sensors. Peng *et al.*, demonstrated a PCF SPR temperature sensor by filling a liquid material into the air holes of the second layer and coating gold film on the inner surface of some of those air holes [5]. Chen *et al.*, reported a fiber SPR temperature sensor, in which the temperature sensitive material was filled into one of cladding air holes [6]. Hameed *et al.*, designed a temperature sensor based on the nematic liquid crystal (NLC)-PCF with an ultrahigh sensitivity [7]. Two electrodes were designed to make sure that the rotation angle of the director of NLC molecules is 90°, by which means it is a complex sensor structure. However, there is a problem on the PCF temperature sensor contacting with single-mode fiber (SMF); besides, the methods of selective filling and coating are complex as well.

In this paper, we design and demonstrate a novel high temperature sensitivity *D*-shaped hole double-cladding fiber (DCF) sensor based on SPR, in which there is a *D*-shaped hole DCF and the gold is well selected as the attractive gold material to SPR. The problem of liquid-sealed in a capillary for a no-hole fiber sensor is saved and a more compact structure is obtained, because the liquid is filled into the *D*-shaped hole. Moreover, in the numerical simulations, the transmission properties of the *D*-shaped hole double-cladding fiber are calculated by a full vector finite element method. The influences of distance between the *D*-shaped hole and fiber core and the thickness of the gold film are investigated to optimize the fiber sensor. Optimizing the *D*-shaped hole double-cladding fiber SPR temperature sensor, the sensitivity can be up to −3.635 nm/°C, which is higher than other reported fiber temperature sensors, such as the side-polished SMF sensor [8], fiber grating sensor [1], fiber Fabry–Perot interferometer sensor [3], multimode interference fiber sensor [2], and PCF sensor based on SPR [5,6].

2. SCHEMATIC AND THEORY

The cross section of fiber temperature sensor based on SPR is shown in Fig. 1. In the fiber sensor, a hollow *D*-shaped section is close to the fiber core. The distance between the hollow *D*-section and fiber core is described by r_d. In order to excite the metal surface plasmon, the gold film is deposited on the inner surface of the *D*-shaped hole with the thickness of h_{Au}. The radius of core, inner cladding, and silica cladding are $r_1 = 5$ μm, $r_2 = 25$ μm, and $r_3 = 62.5$ μm, respectively. Moreover, the refractive index of the core, inner cladding, and silica cladding are defined as n_1 (1.4681), n_2 (1.4628), and n_3 (1.444), respectively.

In the simulations, the complex relative permittivity of the gold is demonstrated by the Drude model, which is expressed as [5]

$$\varepsilon_{Au}(T) = \varepsilon_\infty - \frac{\omega_d(T)^2}{\omega^2 - \omega\omega_c(T)i}, \tag{1}$$

where $\varepsilon_{Au}(T)$ is the permittivity of the gold; ε_∞ represents the permittivity in high frequency; and $\omega_d(T)$ and $\omega_c(T)$ stand for the plasma frequency and damping frequency, respectively. It is also worth noting that the thickness of the gold film is related to temperature. Furthermore, the dispersion of silica is characterized by the Sellmeier equation [9]; the thermo-optic coefficient and expansion coefficient of pure silica can be set to 7.8×10^{-6}/°C and 4.1×10^{-7}/°C, respectively [10]. Assuming the thermo-optic coefficient as dn/dT, the relationship between the refractive index of filled liquid and temperature can be evaluated by [5]

$$n_{\text{det}} = n_{\text{det}\,0} + (T - T_0)dn/dT, \tag{2}$$

where the $n_{\text{det}\,0}$ is the refractive index of filled liquid at the room temperature of T_0. In the proposed fiber SPR sensor, the material dispersion of filled liquid material is neglected. The filled material is the mixture of ethanol ($n_e = 1.3605$) and glycerin ($n_g = 1.4746$) with the thermo-optic coefficient of ethanol and glycerin of -3.94×10^{-4} and -2.15×10^{-4}/°C, respectively [11,12]. The ethanol–glycerin mixture with the refractive index of 1.436 and thermo-optic coefficient of -2.8×10^{-4}/°C can be obtained when the proportions of ethanol and glycerin are 34% and 66%, respectively. From Eq. (2), due to the thermo-optic effects, the refractive index of filled liquid is changed by controlling the temperature, resulting in the resonant coupling phenomenon appearing at other wavelengths. As one very important parameter of the *D*-shaped hole DCF SPR temperature sensor, the temperature sensitivity determines the sensing characteristic, and it can be given by

$$S_\lambda = \frac{d\lambda_{\text{res}}(T)}{dT}[\text{nm/°C}], \tag{3}$$

where λ_{res} is the resonant wavelength of the fiber sensor.

3. SIMULATIONS AND ANALYSIS

Figures 2(a) and 2(b) show the electric field distribution of the *y* and *x* polarizations when the temperature, r_d, h_{Au}, $n_{\text{det}\,0}$, and thermo-optic coefficient of the liquid are 25°C, 5 μm, 47 nm, 1.436, and -2.8×10^{-4}/°C, respectively, and the other parameters are the same as in Fig. 1. In Figs. 2(a) and 2(b), the red arrows stand for the electric vector of the surface plasma wave (SPW). Comparing Figs. 2(a) and 2(b), it can be found that the first-order SPP mode appears at the interface of Au and liquid in the *y*-polarized direction. Moreover, the electric field intensity of *y* polarization in the fiber core is weaker than that of *x* polarization, because the first-order fiber core mode of *y* polarization couples into the same order SPP mode.

The coupling effect with unchanged parameters is shown in Fig. 3. Figure 3 plots the real part of the effective refractive index of the fiber core mode of *y* polarization ($\text{Re}(n_{\text{eff}})$), that of the first-order SPP mode ($\text{Re}(n_{\text{spp}})$) with different wavelengths, and the loss spectrum of the *D*-shaped hole double-cladding fiber SPR temperature sensor. As shown in Fig. 3, the red dashed line for $\text{Re}(n_{\text{spp}})$ declines linearly, while the black solid line for $\text{Re}(n_{\text{eff}})$ exhibits an *S*-shaped kink. For the *D*-shaped hole DCF, the electromagnetic field reveals more into the cladding as the wavelength increases, which leads to the diminution of $\text{Re}(n_{\text{eff}})$. However, with the appearance of resonance, the free electrons and electromagnetic field will

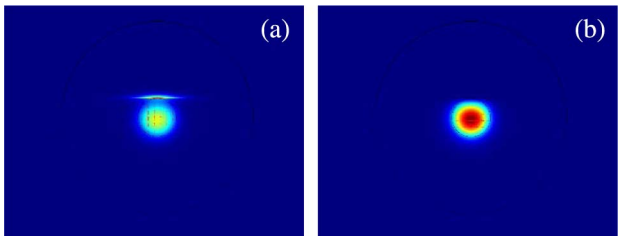

Fig. 2. Electric field distribution (a) of *y* polarization and (b) of *x* polarization.

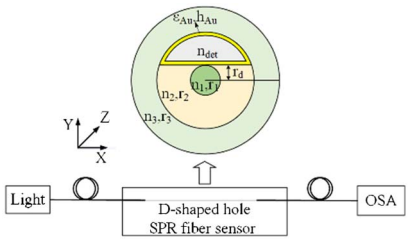

Fig. 1. Cross section of *D*-shaped hole double-cladding fiber SPR temperature sensor and the proposed setup for loss spectrum interrogation.

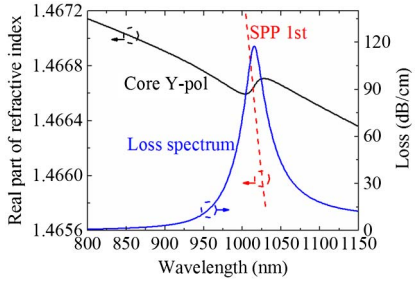

Fig. 3. Real part of effective refractive index of fiber core mode and SPP mode and the loss spectrum of fiber SPR sensor.

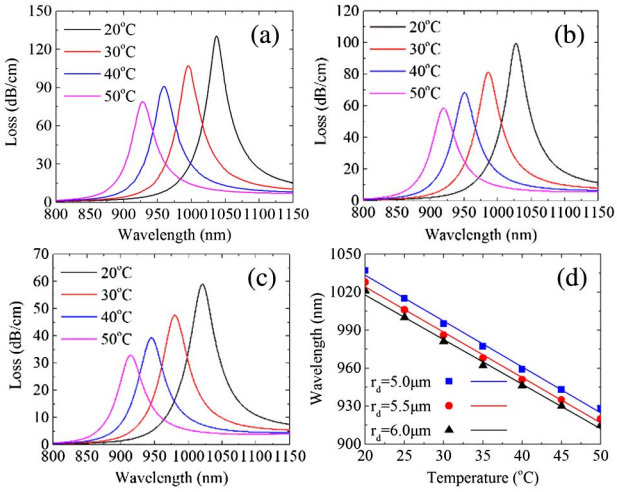

Fig. 4. Influence of r_d on the loss spectrum. (a) $r_d = 5$ μm, (b) $r_d = 5.5$ μm, (c) $r_d = 6$ μm, and (d) the fitted results of resonant wavelength of y polarization with different temperatures, where the blue, red, and black markers are the simulation results.

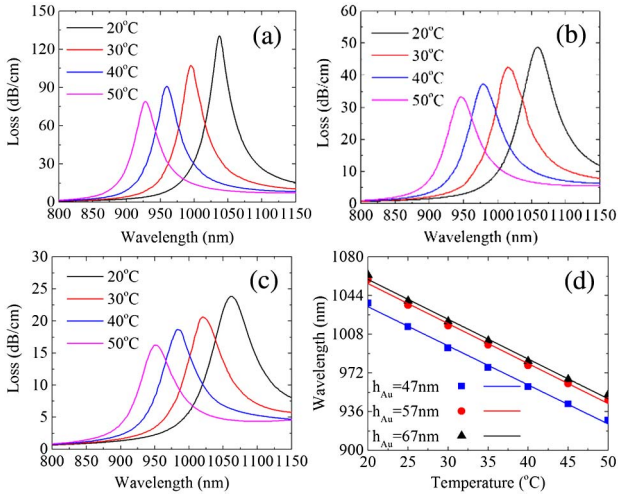

Fig. 5. Influence of h_{Au} on the loss spectrum. (a) $h_{Au} = 47$ nm, (b) $h_{Au} = 57$ nm, (c) $h_{Au} = 67$ nm, and (d) the fitted results of resonant wavelength of y polarization with different temperatures, where the blue, red, and black markers are the simulation results.

be influenced by the evanescent field and oscillation of resonant electrons, respectively, leading to the change of fiber core mode. The electromagnetic field on the left of the resonant wavelength, which is called the slow electromagnetic field, is accelerated by the resonance, while the electromagnetic field on the right of the resonant wavelength, which is named the fast electromagnetic field, is decelerated by the resonance. Therefore, an *S*-shaped kink for $\mathrm{Re}(n_{\mathrm{eff}})$ appears at around the resonant wavelength [13]. The first-order fiber core mode resonantly couples into the same order SPPs mode at the wavelength of 1015 nm, where $\mathrm{Re}(n_{\mathrm{eff}})$ is equal to $\mathrm{Re}(n_{\mathrm{spp}})$. Correspondingly, the loss is up to the maximum at the wavelength of 1015 nm, as shown by the blue solid line.

The distance (r_d) between the fiber core and the *D*-shaped hole is introduced to optimize the *D*-shaped hole double-cladding fiber SPR temperature sensor. Figure 4 shows the influences of r_d with different temperatures. Figures 4(a)–4(c) plot the loss spectra of the *D*-shaped hole double-cladding fiber SPR temperature sensor with the r_d of 5, 5.5, and 6 μm, respectively, when the other parameters remain unchanged. In Fig. 4(a)–4(c), the resonant wavelength moves to shorter wavelengths, and the peaking loss decreases as the temperature increases. When the temperature is 20°C, the peaking loss at the resonant wavelengths of 1037 nm ($r_d = 5$ μm), 1027 nm ($r_d = 5.5$ μm), and 1021 nm ($r_d = 6$ μm) are 130.604, 99.571, and 58.975 dB/cm, respectively. Obviously, the resonant wavelength moves to shorter wavelengths and the peak loss decreases strongly when r_d is increased. This is mainly because the gold film gets closer to the fiber core as r_d keeps decreasing, enhancing the plasmonic wave. The resonant wavelengths with different temperatures are plotted and fitted in Fig. 4(d). In Fig. 4(d), the blue, red, and black solid lines stand for the fitted lines of resonant wavelength corresponding to the r_d of 5, 5.5, and 6 μm, respectively. As plotted in Fig. 4(d), the fitted lines display a good linear fitting. When the r_d are 5, 5.5, and 6 μm, the temperature sensitivities are −3.635, −3.578, and −3.521 nm/°C, respectively. Therefore, the peaking loss is hugely influenced by r_d, while the temperature sensitivity of the fiber SPR sensor is almost unchanged. The main factor considered in the design of r_d is the length of the fiber sensor. In this paper, we set r_d as 5 μm to obtain a better temperature sensitivity and smaller fiber length. When the length of the fiber is about 2 mm, the loss of the fiber is enough for the light detection of the fiber sensor.

The effect of the thickness of gold film (h_{Au}) on the fiber SPR temperature sensor is also discussed. Figure 5 shows the influences on h_{Au} of different temperatures, while the other parameters remain unchanged. Figures 5(a)–5(c) plot the loss spectra of the *D*-shaped hole double-cladding fiber SPR temperature sensor when the h_{Au} is 47, 57, and 67 nm, respectively. As shown in Fig. 5(a)–5(c), the resonant wavelength has blueshift, and the peaking loss decreases with the increase of temperature. Furthermore, when the temperature is selected as 20°C, the peaking loss is 130.604 dB/cm at the resonant wavelength of 1037 nm with the h_{Au} of 47 nm, while the peaking loss decreases to 48.833 dB/cm and the resonant wavelength moves to 1059 nm as the h_{Au} increases to 57 nm; additionally, when the h_{Au} is up to 67 nm, the peaking loss and resonant wavelength are 23.837 dB/cm and 1063 nm, respectively. It is clear that the resonant wavelength moves to longer wavelengths and the peaking loss decreases drastically when the h_{Au} increases from 47 to 67 nm. The drastic decrease of peaking loss is mainly because the penetration distance of the leakage mode of the fiber core is increased with the thickening of the gold film, which leads to a weaker intensity of the SPPs mode at the interface of the Au and liquid. The relationship between the resonant wavelength and temperature with different h_{Au} is shown in Fig. 5(d), where the blue, red, and black solid lines represent the fitted line of the resonant wavelength with different temperatures when the h_{Au} is 47, 57, and 67 nm, respectively. In Fig. 5(d), the fitted lines of the blue, red, and black solid lines decrease linearly, and the slopes of these fitted

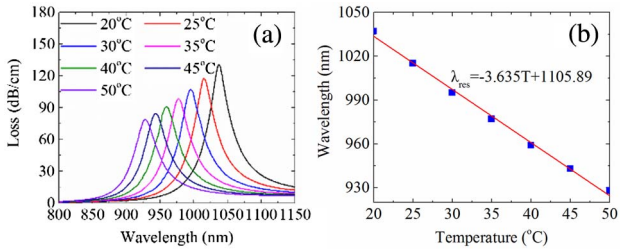

Fig. 6. (a) Loss spectra with different temperatures of y polarization and (b) fitted result of resonant wavelength with different temperatures, where the blue squares are the simulation results and the red line represents the fitted line.

lines are −3.635, −3.720, and −3.701, respectively. Therefore, the peaking loss is greatly affected by the h_{Au}, while the temperature sensitivity of such a fiber sensor varies within a small range. The main factor considered in the choice of h_{Au} is the length of the D-shaped hole fiber sensor. The h_{Au} is selected as 47 nm to get a good temperature sensitivity; meanwhile, the loss is larger than that for other h_{Au}. Similarly, when the length of the fiber is about 2 mm, the loss of the fiber is enough for the light detection of the fiber sensor.

The loss spectra of the D-shaped hole double-cladding fiber SPR sensor with different temperatures are illustrated in Fig. 6(a). In Fig. 6, the r_d and h_{Au} are set as 5 μm and 47 nm while other parameters are unchanged. In Fig. 6(a), the peaking loss is 130.604 dB/cm at the resonant wavelength of 1037 nm when the temperature is 20°C, while the peaking loss decreases to 78.996 dB/cm and the resonant wavelength shifts to 928 nm when the temperature becomes 50°C. This shows that the peaking loss decreases and the resonant wavelength moves to shorter wavelengths with increasing temperature. The resonant wavelengths with different temperatures are fitted and plotted in Fig. 6(b). As plotted in Fig. 6(b), the resonant wavelength almost shows a linear decrease with the increase of temperature, and the sensitivity of the D-shaped hole fiber SPR temperature sensor can reach to −3.635 nm/°C.

For the fiber sensor, the substrate is a D-shaped hole double-cladding fiber. According to Li *et al.* [14], the D-shaped hole double-cladding fiber can be fabricated by using a conventional modified chemical vapor deposition. At first, a D-shaped preform with the refractive index of n_1 (fiber core) and n_2 (inner cladding) can be fabricated. The distance between the fiber core and the hollow D-section is relevant to the structure parameters of the D-shaped preform. In order to fabricate a precise D-shaped preform, the D-shaped preform with a rough cut is polished and stopped several times to measure the residual diameter during the polishing. Then we clear the D-shaped preform and select an appropriate tube with the refractive index of n_3 (the outer cladding). It is worth noting that during the drawing of fiber, the inert gas replaces the low melting point metal which is pumped into the D-shaped hole to obtain a D-shaped hole double-cladding fiber. When the temperature and rate of drawing is reasonable, a good D-shaped hole double-cladding fiber is fabricated. Furthermore, according to the research reported by Sazio and Badding [15] and Baril *et al.* [16,17], the smooth gold film can be deposited on the inner surface of the air hole of a microstructured fiber by high pressure chemical deposition. According to the line of deposit rate, the thickness of the deposited film can be controlled accurately by controlling the deposition time. Therefore, the gold film can be coated on the inner surface of the D-shaped hole in our proposed fiber sensor.

4. CONCLUSIONS

In conclusion, a novel high sensitivity D-shaped hole double-cladding fiber SPR temperature sensor with liquid filling is designed and analyzed. In the fiber sensor, the refractive index of the filled liquid decreases as the temperature increases, leading to the blueshift of the resonant wavelength. Moreover, the r_d and h_{Au} are optimized to obtain a fiber SPR sensor with a temperature sensitivity of −3.635 nm/°C. The research on the SPR temperature sensor based on a D-shaped hole double-cladding fiber with liquid filling would be very useful in the design of novel types of temperature sensor. Moreover, a filled liquid material, which leads to a wider temperature range and higher temperature sensitivity, will be researched in the future.

Funding. National Natural Science Foundation of China (NSFC) (61525501).

REFERENCES

1. J. L. Kou, S. J. Qiu, F. Xu, and Y. Q. Lu, "Demonstration of a compact temperature sensor based on first-order Bragg grating in a tapered fiber probe," Opt. Express **19**, 18452–18457 (2011).
2. Y. Geng, X. Li, X. Tan, Y. Deng, and Y. Yu, "High-sensitivity Mach–Zehnder interferometric temperature fiber sensor based on a waist-enlarged fusion bitaper," IEEE Sens. J. **11**, 2891–2894 (2011).
3. C.-L. Lee, L.-H. Lee, H.-E. Hwang, and J.-M. Hsu, "Highly sensitive air-gap fiber Fabry–Perot interferometers based on polymer-filled hollow core fibers," IEEE Photon. Technol. Lett. **24**, 149–151 (2012).
4. S.-j. Qiu, Y. Chen, F. Xu, and Y.-q. Lu, "Temperature sensor based on an isopropanol-sealed photonic crystal fiber in-line interferometer with enhanced refractive index sensitivity," Opt. Lett. **37**, 863–865 (2012).
5. Y. Peng, J. Hou, Z. Huang, and Q. Lu, "Temperature sensor based on surface plasmon resonance within selectively coated photonic crystal fiber," Appl. Opt. **51**, 6361–6367 (2012).
6. H. Chen, S. Li, J. Li, and Y. Han, "High sensitivity of temperature sensor based on ultracompact photonics crystal fibers," IEEE Photon. J. **6**, 1–6 (2014).
7. M. F. O. Hameed, M. Y. Azab, A. M. Heikal, and S. M. El-Hefnawy, "Highly sensitive plasmonic photonic crystal temperature sensor filled with liquid crystal," IEEE Photon. Technol. Lett. **28**, 59–62 (2016).
8. W.-G. Jung, S.-W. Kim, K.-T. Kim, E.-S. Kim, and S.-W. Kang, "High-sensitivity temperature sensor using a side-polished single-mode fiber covered with the polymer planar waveguide," IEEE Photon. Technol. Lett. **13**, 1209–1211 (2001).
9. G. Agrawal, "Nonlinear fiber optics," in *Nonlinear Science at the Dawn of the 21st Century*, P. L. Christiansen, M. P. Sørensen, and A. C. Scott, eds. (Springer, 2000), pp. 195–211.
10. X. Shu, L. Zhang, and I. Bennion, "Sensitivity characteristics of long-period fiber gratings," J. Lightwave Technol. **20**, 255–266 (2002).
11. R. Yang, Y. S. Yu, Y. Xue, C. Chen, C. Wang, F. Zhu, B. L. Zhang, Q. D. Chen, and H. B. Sun, "A highly sensitive temperature sensor based on a liquid-sealed S-tapered fiber," IEEE Photon. Technol. Lett. **25**, 829–832 (2013).
12. Y. Yu, X. Li, X. Hong, Y. Deng, K. Song, Y. Geng, H. Wei, and W. Tong, "Some features of the photonic crystal fiber temperature sensor with liquid ethanol filling," Opt. Express **18**, 15383–15388 (2010).
13. Z. Tan, X. Hao, Y. Shao, Y. Chen, X. Li, and P. Fan, "Phase modulation and structural effects in a D-shaped all-solid

photonic crystal fiber surface plasmon resonance sensor," Opt. Express **22**, 15049–15063 (2014).
14. L. Li, G. Wylangowski, D. N. Payne, and R. D. Birch, "Broadband metal/glass single-mode fibre polarisers," Electron. Lett. **22**, 1020–1022 (1986).
15. P. J. A. Sazio and J. V. Badding, "Microstructured optical fibers as high-pressure microfluidic reactors," Science **311**, 1583–1586 (2006).
16. N. F. Baril, "High-pressure microfluidic chemical deposition: replacing the air within microstructured optical fibers," dissertations, Doctor of Philosophy (Electronic Theses and Dissertations for Graduate School, 2008).
17. N. F. Baril, R. He, T. D. Day, J. R. Sparks, B. Keshavarzi, M. Krishnamurthi, A. Borhan, V. Gopalan, A. C. Peacock, and N. Healy, "Confined high-pressure chemical deposition of hydrogenated amorphous silicon," J. Am. Chem. Soc. **134**, 19–22 (2012).